Article

Developmental Cell

A Negative Regulatory Mechanism Involving 14-3-3ζ Limits Signaling Downstream of ROCK to Regulate Tissue Stiffness in Epidermal Homeostasis

Graphical Abstract

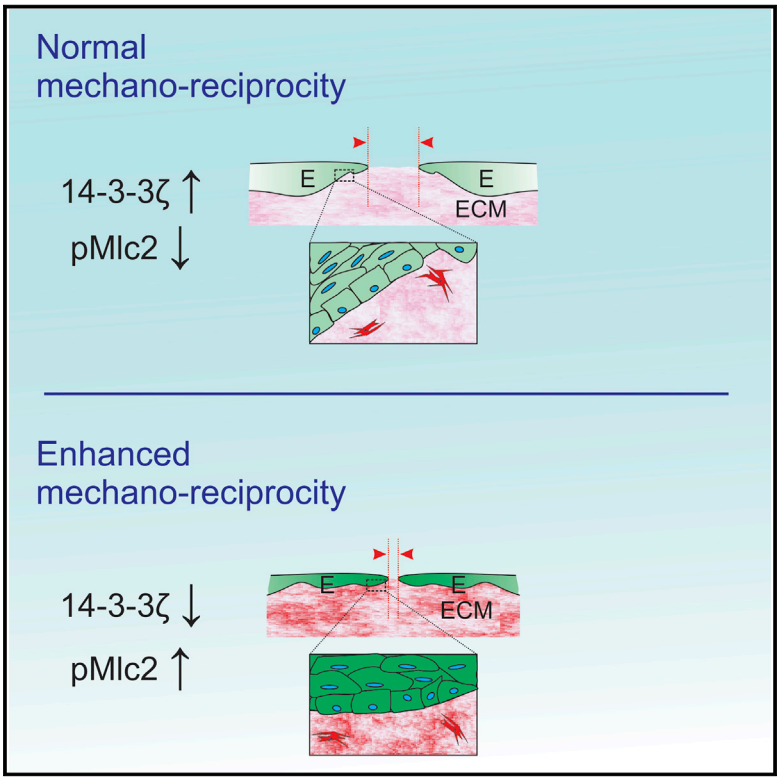

Authors

Jasreen Kular, Kaitlin G. Scheer, Natasha T. Pyne, ..., Hayley S. Ramshaw, Angel F. Lopez, Michael S. Samuel

Correspondence

michael.samuel@unisa.edu.au

In Brief

ROCK signaling increases dermal stiffness by inside-out mechanical signaling. Resulting integrin ligation further activates ROCK by outside-in signaling, establishing a mechano-reciprocal vicious cycle. Kular, Scheer et al. show that in a negative feedback mechanism, 14-3-3ζ limits ROCK signaling in the skin and moderates mechano-reciprocity, with implications for healing and cancer.

Highlights

- 14-3-3ζ deficiency or inhibition enhances signaling flux through ROCK
- Increased signaling via ROCK boosts mechano-reciprocity, accelerating wound healing
- 14-3-3ζ binds Mypt1, promoting its function and enhancing pMlc dephosphorylation
- 14-3-3ζ deficiency increases tumor size

Kular et al., 2015, Developmental Cell *35*, 759–774
December 21, 2015
http://dx.doi.org/10.1016/j.devcel.2015.11.026

CellPress

Developmental Cell
Article

A Negative Regulatory Mechanism Involving 14-3-3ζ Limits Signaling Downstream of ROCK to Regulate Tissue Stiffness in Epidermal Homeostasis

Jasreen Kular,[1,5] Kaitlin G. Scheer,[1,5] Natasha T. Pyne,[1] Amr H. Allam,[2] Anthony N. Pollard,[1] Astrid Magenau,[2] Rebecca L. Wright,[1] Natasha Kolesnikoff,[1] Paul A. Moretti,[1] Lena Wullkopf,[2] Frank C. Stomski,[1] Allison J. Cowin,[3] Joanna M. Woodcock,[1] Michele A. Grimbaldeston,[1,4] Stuart M. Pitson,[1,4] Paul Timpson,[2] Hayley S. Ramshaw,[1,4] Angel F. Lopez,[1,4] and Michael S. Samuel[1,4,*]

[1]Centre for Cancer Biology, SA Pathology and the University of South Australia, Frome Road, Adelaide 5000, Australia
[2]The Kinghorn Cancer Centre & Garvan Institute of Medical Research and St. Vincent's Clinical School, Victoria Street, Darlinghurst, NSW 2010, Australia
[3]Future Industries Institute, University of South Australia, Mawson Lakes 5095, Australia
[4]Faculty of Health Sciences, School of Medicine, University of Adelaide, Adelaide 5000, Australia
[5]Co-first author
*Correspondence: michael.samuel@unisa.edu.au
http://dx.doi.org/10.1016/j.devcel.2015.11.026

SUMMARY

ROCK signaling causes epidermal hyper-proliferation by increasing ECM production, elevating dermal stiffness, and enhancing Fak-mediated mechano-transduction signaling. Elevated dermal stiffness in turn causes ROCK activation, establishing mechano-reciprocity, a positive feedback loop that can promote tumors. We have identified a negative feedback mechanism that limits excessive ROCK signaling during wound healing and is lost in squamous cell carcinomas (SCCs). Signal flux through ROCK was selectively tuned down by increased levels of 14-3-3ζ, which interacted with Mypt1, a ROCK signaling antagonist. In 14-3-3ζ$^{-/-}$ mice, unrestrained ROCK signaling at wound margins elevated ECM production and reduced ECM remodeling, increasing dermal stiffness and causing rapid wound healing. Conversely, 14-3-3ζ deficiency enhanced cutaneous SCC size. Significantly, inhibiting 14-3-3ζ with a novel pharmacological agent accelerated wound healing 2-fold. Patient samples of chronic non-healing wounds overexpressed 14-3-3ζ, while cutaneous SCCs had reduced 14-3-3ζ. These results reveal a novel 14-3-3ζ-dependent mechanism that negatively regulates mechano-reciprocity, suggesting new therapeutic opportunities.

INTRODUCTION

The significance of mechanical force in regulating skin homeostasis is becoming increasingly evident and has important implications for human health (Wong et al., 2012). However, the molecular mechanisms underlying the interplay between mechanical force and cell signaling are poorly understood. A key concept of tissue biology is that increased extra-cellular matrix (ECM) stiffness causes mitogenic signaling that promotes cell proliferation and RhoA activation, or outside-in mechanical signaling (Butcher et al., 2009). Conversely, activation of ROCK, a serine/threonine kinase and the major effector protein of RhoA, causes epidermal proliferation by promoting ECM production and increasing matrix stiffness, or inside-out mechanical signaling (Ibbetson et al., 2013; Samuel et al., 2011a). These two signaling paradigms, termed mechano-reciprocity, balance tissue and cell level forces against each other to maintain tissue and cell integrity. The Rho-ROCK signaling pathway therefore lies at the interface between mechanical and biochemical signaling in skin and other tissues, including mammary (Calvo et al., 2013), ovary (McGrail et al., 2014), and intestine (Haydont et al., 2007). In cutaneous squamous cell carcinoma (SCC), mechano-reciprocity causes a vicious cycle of ever escalating ECM stiffness, ROCK pathway activation, and uncontrolled cell proliferation (Ibbetson et al., 2013; Samuel et al., 2011a). However, during normal re-epithelialization, such as wound healing, re-establishing mechano-reciprocity does not cause uncontrolled cell proliferation, suggesting that negative regulators are deployed under such conditions.

ROCK signaling establishes and regulates the contractility of a trans-cellular actomyosin ring at the wound margin (termed the purse-string mechanism) in the late stage of wound healing (Cowin et al., 2003). However, given the fundamental role of ROCK signaling in ECM homeostasis, it likely functions throughout wound healing in re-establishing mechano-reciprocity, not just in the final stages. Indeed, the re-establishment of mechano-reciprocity has been proposed as a key mechanism guiding wound healing (Schultz et al., 2011), but definitive proof has remained elusive.

14-3-3ζ belongs to a family of highly conserved, acidic, phospho-serine binding proteins (β, γ, ε, σ, ζ, τ, and η) (Ichimura et al., 1988; Toker et al., 1992) that are key players in many cellular processes (Aitken, 2006). Whereas 14-3-3 proteins share considerable sequence homology at the protein level and are thought to act redundantly, there is increasing evidence for non-redundant

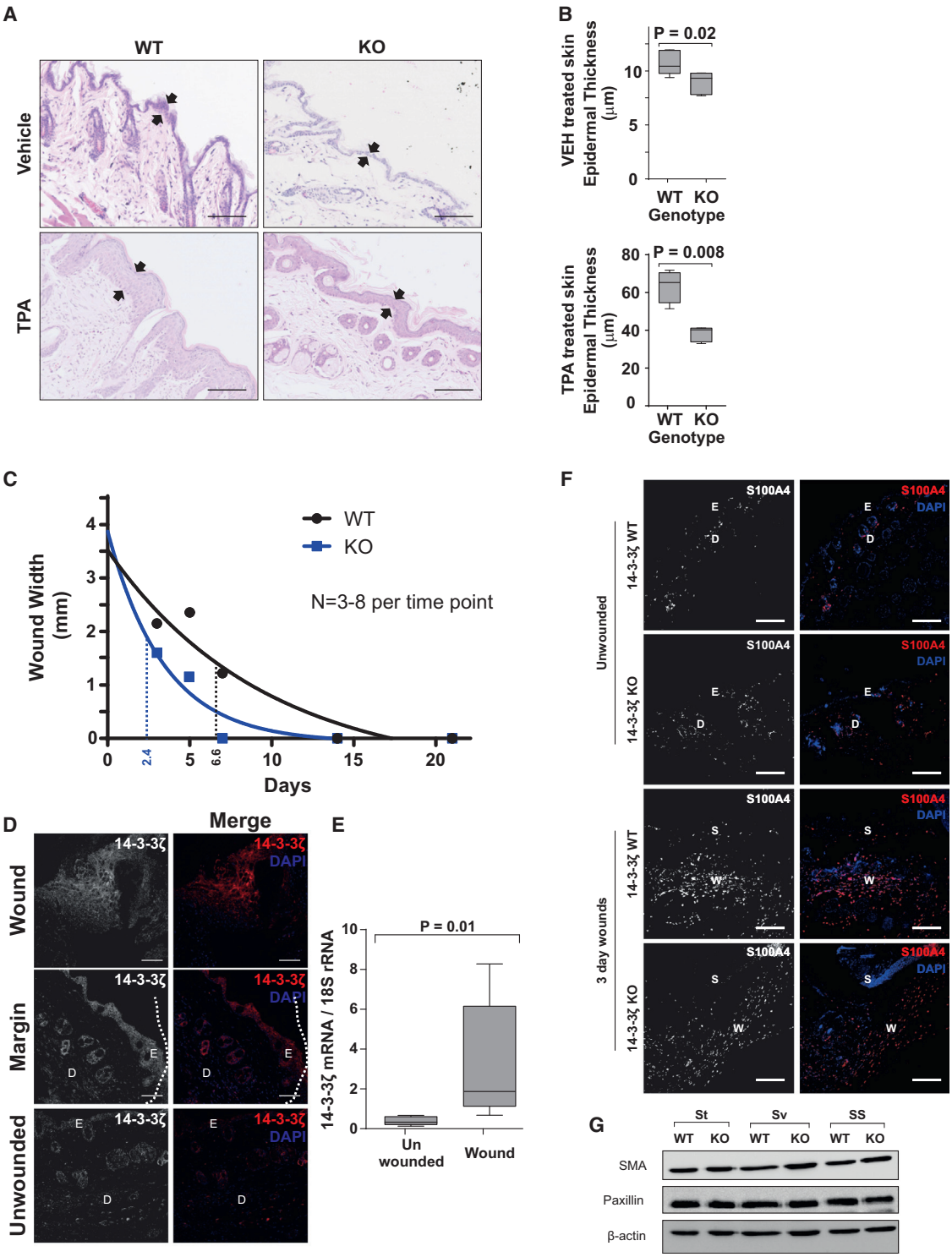

Figure 1. 14-3-3ζ Mice Exhibit Abnormal Epidermal Homeostasis and Rapid Wound Healing

(A and B) Bright-field image of H&E-stained sections of WT and 14-3-3ζ KO skin treated with either vehicle or TPA (A). Epidermal thickness measurements are shown in (B). The scale bar represents 100 μm.

(C) Regression analysis of wound width over time in WT (black circles and line) and 14-3-3ζ KO (blue squares and line) skin. Dotted lines indicate half-times. See Figure S1D for representative images used for measurements.

(D) 14-3-3ζ immunofluorescence (white in single channel, red in merged) in wounds, wound margins (day 5), and intact skin of WT mice. D, dermis; E, epidermis. The scale bars represent 100 μm.

(E) qRT-PCR analysis of 14-3-3ζ mRNA in wounded (day 5) and unwounded skin of WT mice relative to 18S. N = 5.

(legend continued on next page)

functions for individual family members (Cheah et al., 2012; Uhart and Bustos, 2013).

Using mice deficient in 14-3-3ζ and mice expressing conditionally active ROCK, we have revealed a mechanism that moderates mechano-reciprocity, regulates wound healing, and prevents the positively reinforcing cycle of intra- and extracellular forces that promotes tumor progression.

RESULTS

14-3-3ζ Knockout Mice Exhibit Perturbed Epidermal Homeostasis and Accelerated Wound Healing

Optimal balance of cell- and tissue-level forces is needed for tissue homeostasis (Butcher et al., 2009). The skin is exquisitely sensitive to changes in force (Wang et al., 2015). We have previously shown that the balance of extra- and intra-cellular forces is regulated by ROCK signaling and that enhanced mechano-reciprocal forces result in large changes in epidermal thickness (Samuel et al., 2011a). Intriguingly histological analysis of skin biopsies from 14-3-3ζ wild-type (WT) and 14-3-3ζ-deficient (knockout [KO]) mice revealed that KO mice exhibited an ~15% thinner epidermal layer than WT mice (Figures 1A and 1B), and this differential was enhanced to >30% upon epidermal hyper-proliferation induced by topical application of 12-O-tetradecanoylphorbol-13-acetate (TPA), a protein kinase C activator (Niedel et al., 1983) (Figures 1A and 1B). 14-3-3ζ gene-targeted mice had no 14-3-3ζ protein (Figures S1A and S1B) or mRNA (Figure S1C) in the skin and other 14-3-3 isoforms were not differentially regulated in 14-3-3ζ KO skin (Figure S1C), suggesting that 14-3-3ζ has a non-redundant function in epidermal homeostasis.

Because a thin epidermis is reminiscent of impaired mechanical signaling (Samuel and Olson, 2011) in 14-3-3ζ KO skin, we explored if 14-3-3ζ has a role in re-establishing normal mechano-reciprocity during wound repair, using the incisional wound healing model (Lees et al., 2013). 14-3-3ζ KO mice exhibited >2.5-fold faster wound healing compared with WT mice (Figures 1C, S1D, and S1E), with regression analysis showing that the median wound healing time was 2.4 days in 14-3-3ζ KO mice compared with 6.6 days in WT littermates (Figure 1C). At wound margins in WT mice, 14-3-3ζ mRNA and protein levels were elevated compared with those in unwounded WT skin (Figures 1D and 1E), but other isoforms of 14-3-3 were not (Figure S1F), suggesting that 14-3-3ζ has a specific function in wound healing.

To determine if healing of KO wounds was promoted by an increase in dermal fibroblasts, which re-establish the dermal ECM and provide contractile force for wound closure (Driskell and Watt, 2015), we performed immunofluorescence analysis for S100A4/Fsp1 (fibroblast marker; Figure 1F) and α-smooth muscle actin (SMA) (a transient myofibroblast-specific marker; Figure S1G) (Darby et al., 1990) in wounded and unwounded skin but found no differences in the numbers of these cells in the two genotypes at any point in wound healing. Furthermore, SMA levels were comparable in primary dermal fibroblasts from 14-3-3ζ KO and WT mice (Figure 1G; quantified in Figure S1H). These data suggested that rapid wound healing in 14-3-3ζ KO skin was not driven by an increased number of dermal fibroblasts or myofibroblasts.

Rapid Wound Healing in 14-3-3ζ KO Mice Is Associated with Changes in ECM Composition

Normal wound re-epithelialization is dependent on re-establishing the dermis, which comprises ECM populated by dermal fibroblasts and immune cells (Bainbridge, 2013). Dermal fibroblasts produce and remodel the fibrillar ECM proteins (Tomasek et al., 2002). We hypothesized that differences in ECM composition and resulting differences in extra-cellular force may influence wound healing in 14-3-3ζ KO skin. We therefore analyzed collagen composition and remodeling at wound margins by second harmonic generation (SHG) microscopy (Ibbetson et al., 2013; Samuel and Olson, 2011). Area coverage analysis of SHG images revealed more collagen at wound margins in 14-3-3ζ KO skin compared with WT skin at the protein level (Figures 2A and 2B; see also the schematic for wound imaging in Figure S2A), consistent with mRNA expression data (Figure S2B). Furthermore, collagen fibers at 14-3-3ζ KO wound margins appeared less organized than at WT wound margins and lacked the uniformly bundled, parallel structures characteristic of normal dermal collagen (Figure 2A, insets). Accordingly, gray-level co-occurrence matrix (GLCM) analysis performed on SHG images of WT and 14-3-3ζ KO mice 7 days after wounding showed that collagen fibers at 14-3-3ζ KO wound margins have a significantly slower signal decay than in fibers in WT wounds (Figures 2C and S2C), suggesting that 14-3-3ζ KO wounds have a denser, un-remodeled collagen matrix than WT wounds. Similarly, increased levels of two other ECM proteins, periostin (Figures 2D and S2D) and tenascin-C (Figures 2E and S2E), were observed in 14-3-3ζ KO skin compared with WT skin. All three proteins have established functions in tissue regeneration (Kudo, 2011; Midwood et al., 2011). Interestingly, collagen (Figure S2F) and periostin (Figure S2G) levels were similar in unwounded 14-3-3ζ KO and WT skin, and tenascin-C (Figure S2H) was undetectable in unwounded skin of either genotype. Taken together, these results show that 14-3-3ζ deficiency increased ECM production and impaired remodeling at wound margins.

Signaling Downstream of ROCK Is Hyper-activated at Wound Margins in 14-3-3ζ KO Mice

ROCK activation at cutaneous wound margins regulates the assembly and contraction of an actin ring, which facilitates wound closure at the late stages of wound healing (Russo et al., 2005). However, we have also previously shown that ROCK signaling in keratinocytes regulates the production of several ECM proteins strongly linked to mechanical signaling in the dermis

(F) S100A4 immunofluorescence (white in single channel, red in merged) in unwounded skin and day 5 wounds of 14-3-3ζ KO and WT mice. S, scar; W, wound. The scale bars represent 100 μm.

(G) Western analysis of paxillin and SMA in primary dermal fibroblasts cultured under steady-state conditions (St), starved of serum (Sv), or stimulated following starvation (SS) as described in Experimental Procedures.

See also Figure S1.

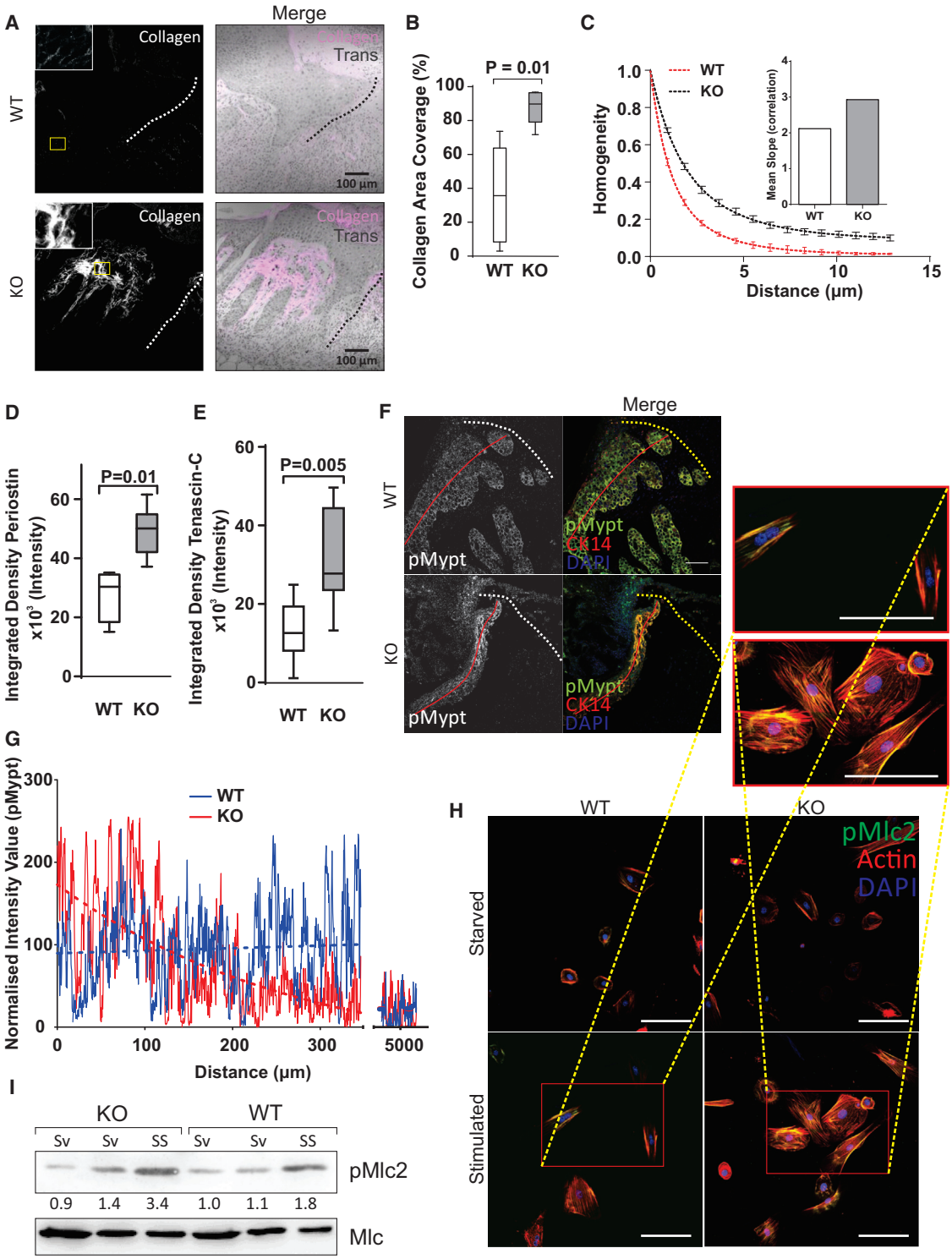

Figure 2. Rapid Wound Healing in 14-3-3ζ KO Mice Is Associated with Changes in ECM Composition and Increased ROCK Signaling

(A and B) Dual two-photon SHG and monochromatic transmission (Trans; grayscale in merge) images showing collagen (white in single channel, magenta in merged) around day 7 wound margins (dotted lines) in H&E-stained WT and 14-3-3ζ KO skin sections (A). Yellow boxes are magnified in insets. Area coverage analysis (10 fields/sample from five mice/genotype) of SHG is quantified in (B).

(C) GLCM analysis of SHG images from WT and 14-3-3ζ KO day 7 wound margins, with signal homogeneity plotted against distance from each reference pixel. Dashed lines show the non-linear bi-exponential fit to each data set. Error bars indicate SEM. Regions analyzed are shown in Figure S2. Inset shows the mean decay parameter (slope) of the bi-exponential fit model of correlation decay curve for samples of each genotype. N = 10.

(legend continued on next page)

(Ibbetson et al., 2013). We hypothesized that ROCK activation at wound margins may also have a role in regulating dermal ECM regeneration and therefore assessed ROCK activation at wound margins in WT and 14-3-3ζ KO mice by confocal immunofluorescence analysis of the myosin phosphatase target subunit 1 phosphorylated (pMypt1) at the ROCK target site Thr-696 (Feng et al., 1999). To delineate the epidermis, we used the keratinocyte marker cytokeratin 14 (CK14). WT mice exhibit a broad band of moderately elevated pMypt1 close to the wound, whereas KO mice exhibit greatly increased pMypt1 at wound margins compared with WT mice throughout the healing process (Figures 2F and 2G). Baseline pMypt1 levels measured 5 mm from the wound edge (Figure 2G) were comparable in both genotypes and similar to those observed under unwounded, steady-state conditions (Figure S2I). Because Mypt1 may also be phosphorylated by other Rac-effector proteins such as Mrck (Wilkinson et al., 2005), we sought to confirm differential ROCK activation in WT and 14-3-3ζ KO cells in vitro. To that end, we derived primary dermal fibroblasts and keratinocytes from WT and 14-3-3ζ KO mice and validated these by fibroblast- and keratinocyte-specific markers, S100A4/Fsp1 and CK14, respectively (Figure S2J). When primary keratinocytes of both genotypes seeded at low density were starved and then treated with 50 ng/ml EGF for 1 hr (time selected by analyzing the time course of signaling; Figure S2K) to stimulate Rho-ROCK pathway activation, 14-3-3ζ KO keratinocytes exhibited significantly increased stress fiber formation compared with WT (Figure 2H and Figure S2L, insets). Mlc2 is activated by Thr-18/Ser-19 di-phosphorylation by ROCK (Amano et al., 1996). We observed increased phosphorylation of regulatory myosin light chain (pMlc2; Figure 2I) localized to stress fibers in 14-3-3ζ KO keratinocytes compared with WT keratinocytes (Figure 2H and Figure S2L, inset). Together, these data suggest that signaling through ROCK is enhanced in 14-3-3ζ KO compared with WT keratinocytes under identical conditions that cause signaling through this pathway, at wound margins and in vitro.

Increased Signaling Downstream of ROCK at 14-3-3ζ KO Wound Margins Accelerates Re-epithelialization by Enhancing Mechano-transduction Signaling

To determine if enforced ROCK activation at wound margins is capable of accelerating re-epithelialization, we used a mouse model (K14-ROCK:ER) that we previously generated, in which ROCK may be conditionally activated in the epidermis by topical application of 4-hydroxytamoxifen (4HT) (Samuel et al., 2009a). Upon ROCK activation at wound margins of K14-ROCK:ER mice, re-epithelialization was accelerated compared with that in K14-KD:ER control mice that express kinase-dead ROCK (Figure 3A), in a statistically significant manner comparable with that observed in 14-3-3ζ KO relative to WT wounds. Accelerated wound healing in K14-ROCK:ER mice was accompanied by increased collagen (Figure 3B), periostin, and tenascin C (Figure 3C) production compared with that in K14-KD:ER mice, very reminiscent of our observations in 14-3-3ζ KO versus WT wounds (Figures 2A, 2B, 2D, and 2E). Taken together with our previous reports that ROCK-mediated ECM deposition and remodeling induces epidermal cell proliferation (Samuel et al., 2011a), these data strongly suggest that ROCK-mediated ECM production is increased in 14-3-3ζ KO wounds.

Because elevated collagen density is associated in many tissues with increased outside-in mechanical signaling mediated by integrin ligation (Egeblad et al., 2010), we next assessed Fak auto-phosphorylation at Tyr-397, a known early response to increased ECM density (Assoian and Klein, 2008). p(Tyr-397)Fak levels were elevated in re-epithelializing K14-ROCK:ER wounds compared with those in K14-KD:ER control wounds (Figure 3D, top panels), strongly suggesting that outside-in mechanical signaling was enhanced under conditions of ROCK activation. Similarly, p(Tyr-397)Fak was also elevated at 14-3-3ζ KO wound margins compared with WT margins (Figure 3E, top panels; quantified in Figure 3F), suggesting that outside-in mechanical signaling was enhanced when 14-3-3ζ was absent. Furthermore, we also observed increased levels of (active) p(Ser-473)Akt in K14-ROCK:ER wounds (Figure 3D, bottom panels) and 14-3-3ζ KO wounds (Figure 3E, bottom panels) compared with K14-KD:ER and WT wounds, respectively, consistent with the activation of mechano-transduction pathways downstream of integrin activation (Tian et al., 2002). These data show that when 14-3-3ζ is absent, the mechano-transduction signaling pathway downstream of integrins and FAK are hyper-activated at wound margins, in a similar manner to that in ROCK-activated wounds.

Together with our previous observations that the collagen → integrin → FAK → PI3K/AKT pathway enhances epidermal proliferation (Samuel et al., 2011a), our new data reveal that 14-3-3ζ has a fundamental role in epidermal homeostasis and wound healing by negatively regulating mechano-reciprocity through a mechanism that inhibits inside-out mechano-transduction signaling pathways mediated by ROCK.

To determine if enhanced signaling through ROCK was responsible for accelerated wound healing in 14-3-3ζ KO mice, we adopted a pharmacological approach, topically applying the selective ROCK inhibitor Y-27632 or vehicle to the wound margins (25 μg/mouse once daily for 5 days) of cohorts of

(D and E) Quantification of periostin (D) and tenascin-C (E) at day 7 WT and 14-3-3ζ KO wound margins by integrated density measurements of immunofluorescence on tissues from four mice/genotype, 10–12 fields/mouse. Representative images: Figures S2D and S2E.

(F) Representative confocal immunofluorescence analysis of phospho-Thr-696 myosin phosphatase (pMypt, white in single channel, green in merged) at 14-3-3ζ KO and WT wound margins. Tracks used for line scans in (G) are shown in red. The scale bar represents 100 μm.

(G) A representative line scan of p(Thr-696)Mypt1 immunofluorescence derived from a WT and a 14-3-3ζ KO wound, showing fluorescence intensity versus distance from margin (solid lines). Mean fluorescence intensity (dotted lines) and fluorescence at a distal site, 5 mm from the wound are also shown (n = 5).

(H) Confocal immunofluorescence analysis of cultured primary 14-3-3ζ KO and WT keratinocytes, starved in serum-free DMEM or starved and then incubated in complete keratinocyte growth medium supplemented with 50 ng/ml EGF for 1 hr, showing actin stress fibers (Actin, red) and co-localized myosin light chain phosphorylated at Ser-19 (pMlc2, green). Red inset is magnified. The scale bar represents 100 μm. See also Figure S2L.

(I) Western analysis of pp(Thr-18/Ser-19)-Mlc2 in cultured primary keratinocytes that have been starved (Sv) or stimulated following starvation (SS). Numbers represent pMlc2 bands intensities normalized to total Mlc.

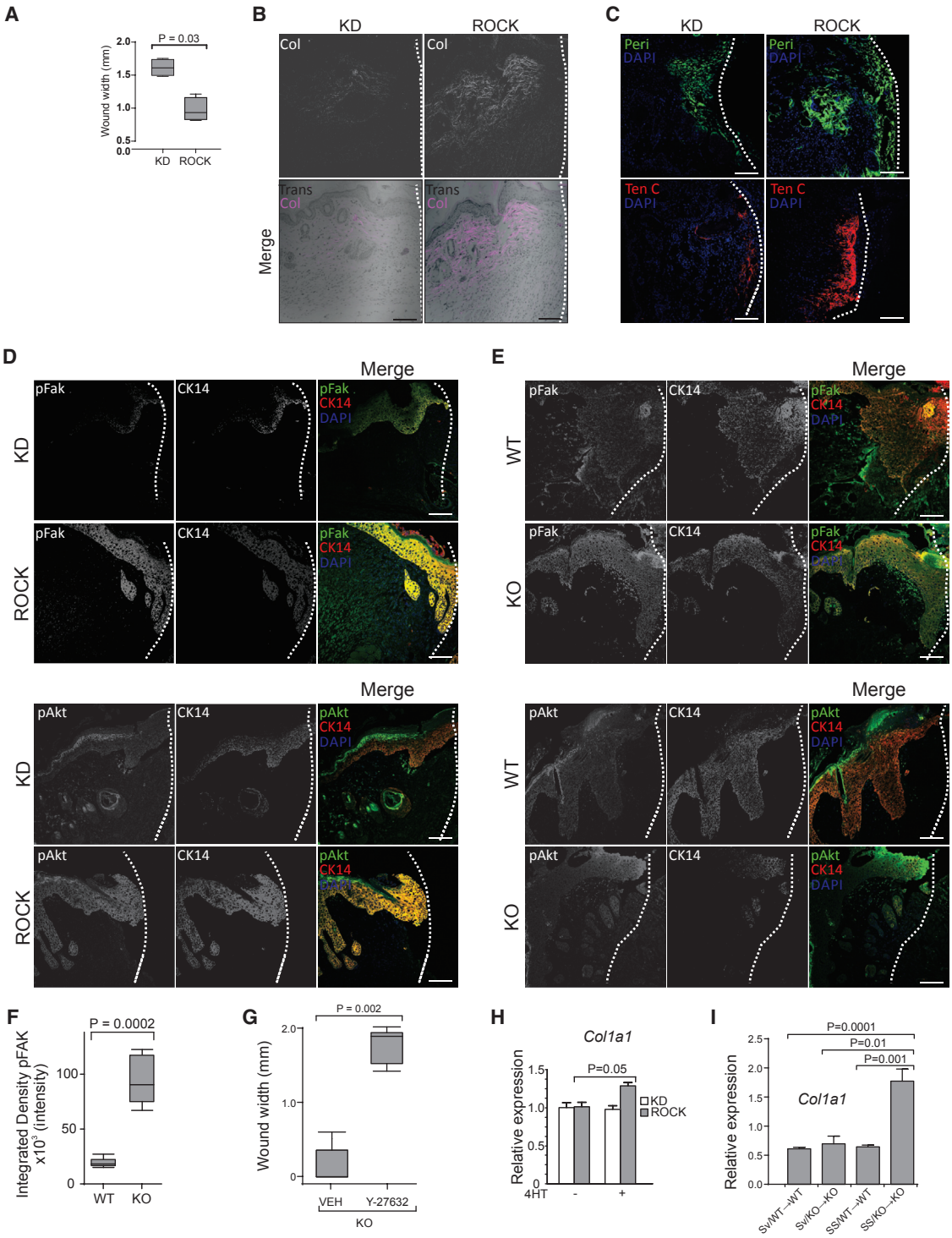

Figure 3. Outside-In Mechano-transduction Signaling Is Enhanced at 14-3-3ζ KO Wound Margins and Is Dependent on ROCK Activity

(A) Wound widths at day 7 following wounding in K14-KD:ER and K14-ROCK:ER mice (four mice/genotype) topically treated daily with 4HT. N = 5.

(B) Two-photon SHG microscopy of collagen (white in single channel, magenta in merged) with co-acquired transmission image (Trans) of H&E-stained sections of K14-KD:ER and K14-ROCK:ER wound margins. The scale bars represent 100 μm.

(C) Confocal immunofluorescence analysis of periostin (Peri; green) and tenascin-C (Ten C; red) at day 7 K14-KD:ER and K14-ROCK:ER wound margins. The scale bars represent 100 μm.

(D) Confocal immunofluorescence analysis of pFak (top six panels: white in single channel, green in merged) and pAkt (bottom six panels: white in single channel, green in merged) at day 7 K14-KD:ER and K14-ROCK:ER wound margins. CK14 denotes epidermal layer. The scale bars represent 100 μm.

(legend continued on next page)

14-3-3ζ KO mice. ROCK inhibition completely abolished accelerated wound healing in 14-3-3ζ KO mice (Figure 3G) and greatly reduced collagen production at wound margins (Figure S3A). These data show that the accelerated wound healing in 14-3-3ζ KO mice is likely mediated by enhanced ECM-initiated mechano-transduction signaling caused by increased ROCK activation at wound margins.

Dermal fibroblasts are the cells mainly responsible for producing ECM proteins (Tomasek et al., 2002). Media conditioned in vitro by ROCK-activated K14-ROCK:ER keratinocytes, induced collagen 1a and 3a mRNA in WT dermal fibroblasts, whereas media conditioned by K14-KD:ER-derived primary keratinocytes did not (Figures 3H and S3B), suggesting that ROCK activation in keratinocytes stimulates collagen production by fibroblasts by a paracrine mechanism. Similarly, media conditioned by 14-3-3ζ KO primary keratinocytes subjected to serum starvation followed by serum stimulation induced >2-fold more transcription of collagen 1a and 3a in primary dermal fibroblasts compared with media conditioned in the same manner by WT keratinocytes (Figures 3I and S3C). Taken together, these data strongly suggest that the accelerated healing of 14-3-3ζ KO wounds is dependent on sharply elevated signaling downstream of ROCK at 14-3-3ζ KO wound margins compared with WT (Figure 2F), which caused increased paracrine signaling to dermal fibroblasts, enhanced ECM production, elevated outside-in mechano-transduction signaling mediated by FAK and Akt, and accelerated re-epithelialization.

14-3-3ζ in Inflammatory Cells Does Not Influence Wound Healing

Inflammation plays a key role in wound healing by fighting infection and clearing tissue debris (Eming et al., 2007). To ascertain if 14-3-3ζ deficiency in the immune cell infiltrate of 14-3-3ζ KO wounds has a role in accelerated healing, we generated bone marrow chimeric mice as follows: WT bone marrow cells engrafted into WT mice as an engraftment control, 14-3-3ζ KO bone marrow cells into WT mice, and conversely WT bone marrow cells into 14-3-3ζ KO mice as test cohorts. After allowing 4 weeks for reconstitution of the immune system, we performed incisional wounding on these mice and measured the widths of wounds harvested at day 5 after wounding. Wound healing in 14-3-3ζ KO mice engrafted with WT bone marrow was significantly accelerated compared with that in WT mice engrafted with 14-3-3ζ KO bone marrow or WT mice engrafted with WT bone marrow (Figure 4A). Engraftment was verified by flow cytometry (Figures S4A and S4B), which also showed that 14-3-3ζ KO inflammatory cells are recruited to wounds at comparable rates to WT inflammatory cells (Figure S4B, skin panel). These data strongly suggest that the 14-3-3ζ deficiency in the immune system plays no role in the accelerated healing of 14-3-3ζ KO wounds.

14-3-3ζ KO Dermal Fibroblasts Exhibit Impaired Matrix Remodeling Capabilities

To determine why impaired collagen remodeling was observed during the healing of 14-3-3ζ KO wounds compared with WT (Figures 2C and S2C), we used primary dermal fibroblasts derived from 14-3-3ζ KO mice and their WT littermates in an in vitro collagen remodeling assay (Nobis et al., 2013; Timpson et al., 2011). WT dermal fibroblasts embedded into a collagen matrix rapidly remodeled the collagen fibers, resulting in a significant reduction in matrix size within 5 days, whereas 14-3-3ζ KO dermal fibroblasts could not (Figure 4B). 14-3-3ζ KO fibroblasts plated onto a collagen matrix exhibited more stress fibers than WT dermal fibroblasts (Figure 4C) reminiscent of 14-3-3ζ KO keratinocytes (Figures 2H and S2L), but also larger focal adhesions that persisted upon serum starvation compared with WT dermal fibroblasts (Figure 4C). However, total paxillin levels were similar in dermal fibroblasts of both genotypes (Figure 1G; quantified in Figure S1H). Live-cell imaging of dermal fibroblasts containing paxillin labeled with eGFP revealed that focal adhesion number and size were increased in 14-3-3ζ KO compared with WT dermal fibroblasts (Movie S1; Figures 4D–4F). Dynamic regulation of focal adhesions such that they are assembled and disassembled in a coordinated fashion is essential to fibroblast motility and their ECM remodeling functions (Calvo et al., 2013; Maller et al., 2013). Accordingly, cell motility on a collagen coated surface as determined by the movement of cells into a scratch wound (Figures 4G, S4C, and S4D) was significantly lower in 14-3-3ζ KO fibroblasts compared with WT fibroblasts. Furthermore, dual live-cell imaging of GFP-labeled dermal fibroblasts with corresponding SHG imaging of 3D organotypic collagen matrices in which the cells had been embedded revealed that whereas WT cells exhibited an elongated, fibroblast-like morphology and actively interacted with the collagen matrix (Movie S2; Figure 4H) consistent with good collagen remodeling capacity (Figure 4B), 14-3-3ζ KO dermal fibroblasts exhibited a contracted morphology with blebbing, consistent with hyper-activated ROCK signaling, did not interact with the collagen matrix, and were relatively immotile (Movie S2; Figure 4H), consistent with poor ECM remodeling capacity (Figure 4B). Circularity analysis of cells in 3D organotypic collagen matrices performed to establish a quantitative basis for cell morphology revealed that 14-3-3ζ KO fibroblasts were approximately 40% less elongated that WT fibroblasts (Figure 4I) but, interestingly, adopted an elongated morphology similar to that of WT fibroblasts when incubated in 3D organotypic collagen matrices containing the selective ROCK inhibitor Y-27632 (Movie

(E) Representative confocal immunofluorescence analysis of pFak (top six panels: white in single channel, green in merged) and pAkt (bottom six panels: white in single channel, green in merged) at day 7 WT and 14-3-3ζ KO wound margins. CK14 denotes epidermal layer. The scale bars represent 100 μm.
(F) Integrated density of pFak immunofluorescence at wound margins of day 7 WT and 14-3-3ζ KO wounds. N = 8.
(G) Widths (day 5) of 14-3-3ζ KO wounds topically treated daily with vehicle (VEH) or ROCK inhibitor (Y-27632). N = 6.
(H) *Col1a1* mRNA expression relative to 18 s rRNA in dermal fibroblasts incubated for 8 hr with medium conditioned for 18 hr by keratinocytes expressing kinase-dead (KD) ROCK or conditionally activated ROCK, diluted 1:1 with fibroblast growth medium. N = 3.
(I) *Col1a1* mRNA expression relative to 18S rRNA in WT or 14-3-3ζ KO primary dermal fibroblasts incubated for 8 hr with medium conditioned for 18 hr by starved (Sv) or starved and stimulated (SS), WT or 14-3-3ζ KO primary keratinocytes, diluted 1:1 with fibroblast growth medium. N = 3.
See also Figure S3.

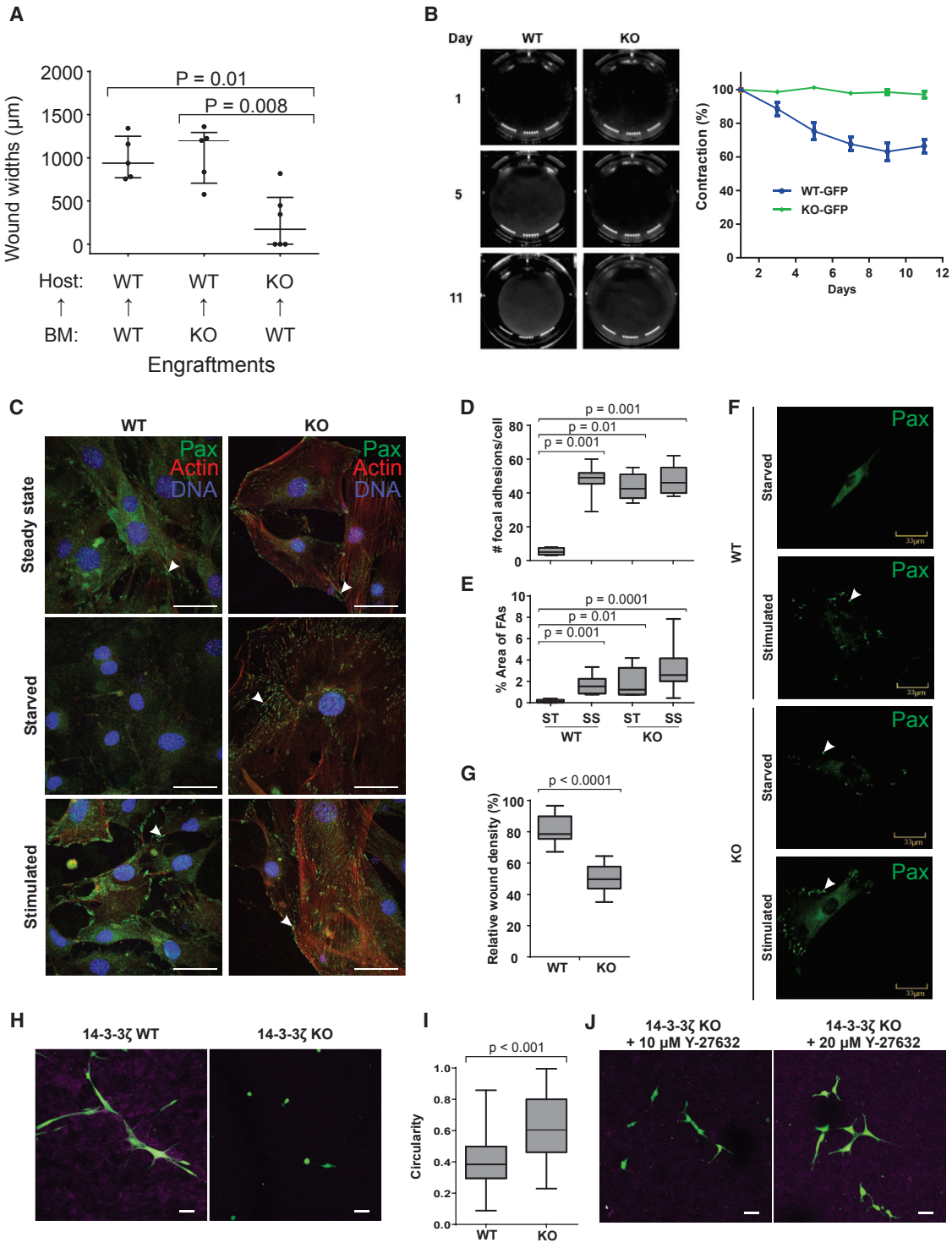

Figure 4. 14-3-3ζ KO Dermal Fibroblasts Exhibit Reduced Matrix Remodeling Capabilities and Motility

(A) Wound widths (day 5) of WT or 14-3-3ζ KO mice that had been reconstituted (↑) with WT or 14-3-3ζ KO bone marrow cells as indicated.

(B) Representative images of collagen matrices containing $0.8x10^6$ WT or 14-3-3ζ KO fibroblasts on days 1, 5, and 11 of culture. Percentage contraction is quantified. N = 3 matrices per condition.

(C) Immunofluorescence analysis of focal adhesions (paxillin [green]) with actin (red) in steady state, serum starved, and starved and stimulated 14-3-3ζ KO and WT primary dermal fibroblasts. Arrowhead indicates a focal adhesion. The scale bar represents 50 µm.

(D) Number of eGFP-paxillin labeled focal adhesions per cell (N = 8–10) from live-cell images of starved or starved and stimulated WT or 14-3-3ζ KO dermal fibroblasts.

(legend continued on next page)

S2; Figure 4J). Tellingly, this effect of Y-27632 was dose dependent.

These results show that 14-3-3ζ deficiency in dermal fibroblasts mediates aberrant focal adhesion dynamics associated with a contracted morphology, reduced capacity to migrate on collagen, and impaired ability to remodel 3D collagen matrices. Collagen remodeling capacity and motility are restored by selective ROCK inhibition, strongly suggesting that increased ROCK activation in 14-3-3ζ KO fibroblasts is the cause of these phenotypes.

Signaling Flux through the ROCK Pathway Is Also Elevated in 14-3-3ζ KO Dermal Fibroblasts

Rho activity mediated by ROCK induces and stabilizes stress fibers and focal adhesions, and Rho inhibition at the leading edge is required for the focal adhesion dynamics essential for cell motility (reviewed by Burridge and Wennerberg, 2004). We therefore hypothesized that 14-3-3ζ deficiency may enhance signaling downstream of ROCK in dermal fibroblasts in a manner similar to that shown above in keratinocytes. Western analysis showed that Mypt1 (particularly the 75 kDa isoform) (Olsen et al., 2010) phosphorylated at ROCK target site Thr-696 (Figure 5A; quantified in Figure 5C), and Mlc2 di-phosphorylated at ROCK target sites Thr18 and Ser19 (Figure 5B; quantified in Figure 5D) were more abundant in 14-3-3ζ KO cells than in WT cells, particularly under conditions in which the ROCK pathway is activated.

These observations show that 14-3-3ζ deficiency causes increased signal flux through the ROCK pathway in dermal fibroblasts and increased phosphorylation of ROCK target proteins.

Mypt1 Phosphorylation at Ser-909 Is Required for Strong Association with 14-3-3ζ

To determine if 14-3-3ζ interacts with signaling proteins associated with the ROCK signaling pathway, we performed pull-down assays using recombinant murine 14-3-3ζ-GST fusion protein on glutathione Sepharose beads, incubated with whole-cell lysates of dermal fibroblasts. Of all the Rho-ROCK signaling proteins predicted to have putative 14-3-3 consensus binding sites (indicated in red in Figure 5E) as identified by Scansite 3.0 (Obenauer et al., 2003), only Mypt1 interacted with 14-3-3ζ (Figure 5F) under these conditions. Furthermore, in dermal fibroblasts that had been starved and stimulated (Figure 5G) as well as in primary WT keratinocytes (Figure 5H), endogenous Mypt1 co-immunoprecipitated with 14-3-3ζ in the presence of phosphatase inhibitors but not in the presence of alkaline phosphatase (Figure 5G, lane $C16_{(P)}$), strongly suggesting that the interaction between 14-3-3ζ and Mypt1 is physiologically relevant and dependent on phosphorylation. Interestingly, co-immunoprecipitation of Mypt1 with 14-3-3ζ was not observed with another 14-3-3 antibody (G1-7) (Ramshaw et al., 2013) with lower selectivity for 14-3-3ζ than for other isoforms (Figure 5G). Taken together with our data showing increased Mlc2 phosphorylation in 14-3-3ζ KO cells (Figures 2H, 5B, and 5D), these results show that 14-3-3ζ strongly associates with Mypt1.

To determine which amino-acid residues were critical for Mypt1's association with 14-3-3ζ, we generated expression constructs encoding FLAG-tagged versions of Mypt1 and carrying S→A modifications at putative 14-3-3ζ binding sites, overexpressed these in HEK293T cells and performed co-immunoprecipitation analysis with an anti-FLAG antibody. Although 14-3-3ζ was capable of associating with $Mypt1^{S445A}$ and $Mypt1^{S472A}$ as readily as it could with WT Mypt1, its association with $Mypt1^{S909A}$ and a version of Mypt1 in which all three serine residues were changed to alanine ($Mypt1^{SiiiA}$) was significantly impaired (Figure 5I; quantified in histogram). We therefore concluded that phosphorylation at Ser-909 is required for the strong association of 14-3-3ζ with Mypt1.

Pharmacological Inhibition of 14-3-3 Function Accelerates Wound Healing and Phenocopies 14-3-3ζ Deficiency

The 14-3-3 proteins function as obligate dimers (Messaritou et al., 2010). 14-3-3 dimerization and therefore function are abolished by phosphorylation at Ser-58, which is located at the dimer interface (Woodcock et al., 2010). We have recently reported the rational design and validation of novel pharmacological inhibitors of 14-3-3 that function by facilitating 14-3-3 phosphorylation at the dimer interface (Woodcock et al., 2015). To determine if 14-3-3 inhibition in the skin phenocopies 14-3-3ζ deficiency and accelerates wound re-epithelialization, we topically treated WT and 14-3-3ζ KO mice with RB-11 at a dose previously shown to inhibit 14-3-3 in vivo (Woodcock et al., 2015), for 7 days following incisional wounding. 14-3-3 inhibition increased the rate of re-epithelialization (Figure 6A), enhanced Mypt1 phosphorylation at wound margins (Figure 6B), and elevated collagen production (Figure 6C) in WT mice, similar to that observed in 14-3-3ζ KO wounds (Figure 2). Furthermore, WT dermal fibroblasts cultured in the presence of RB-11, exhibited reduced collagen remodeling capacity approaching that observed in 14-3-3ζ KO dermal fibroblasts (Figures 6D and S5A). Live-cell images of GFP-labeled WT dermal fibroblasts within 3D collagen organotypic matrices treated with RB-11 exhibited a contracted morphology and interacted with the ECM and each other infrequently in a manner similar to 14-3-3ζ KO fibroblasts that had been treated with RB-11 or vehicle (Movie S2). Circularity

(E) Area of eGFP-paxillin labeled focal adhesions per cell (N = 8–10) in live-cell images of starved or stimulated WT or 14-3-3ζ KO dermal fibroblasts.
(F) Still frames from live-cell movies of starved or stimulated WT or 14-3-3ζ KO dermal fibroblasts, expressing eGFP-paxillin. Arrowhead indicates a focal adhesion. See also Movie S1.
(G) Relative wound density measurements of in vitro scratch wound assays conducted on WT or 14-3-3ζ KO and dermal fibroblast cultures. Results are from three experiments of eight scratch assays per genotype.
(H) Still frames from dual GFP fluorescence (green) and collagen SHG (magenta) live-cell movies of GFP labeled WT and 14-3-3ζ KO dermal fibroblasts in 3D collagen matrices. The scale bars represent 100 μm. See also Movie S2.
(I) Cell circularity of WT and 14-3-3ζ KO dermal fibroblasts cultured in collagen matrices. Data are from three fields containing several hundred cells per condition.
(J) Still frames from dual GFP fluorescence (green) and collagen SHG (magenta) live-cell movies of GFP labeled WT and 14-3-3ζ KO dermal fibroblasts in 3D collagen matrices, cultured with or without Y-27632 (0, 10, or 20 μM). The scale bars represent 100 μm. See also Movie S2.
See also Figure S4.

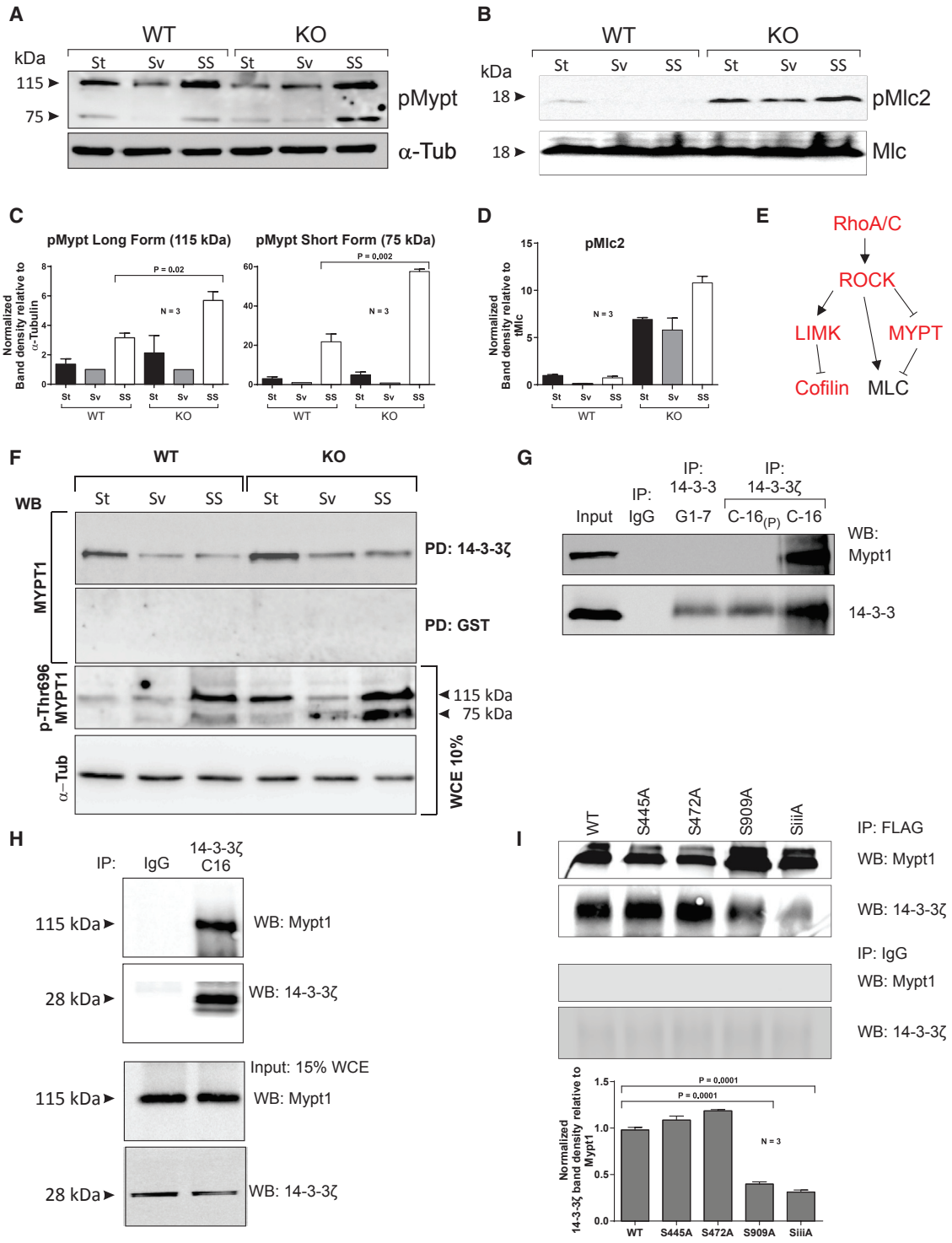

Figure 5. 14-3-3ζ Binds Mypt1 to Regulate Signal Flux Downstream of ROCK

(A and B) Western analysis of WT and 14-3-3ζ KO cultured dermal fibroblasts. Antibodies are indicated on the right. SS, starved for 24 hr and stimulated with medium containing 10% serum for 1 hr; St, standard culture conditions; Sv, starved 24 hr in serum-free medium.

(C) Mean band densities of both the long (115 kDa) and short (75 kDa) forms of p(Thr-696)Mypt1 relative to α-tubulin and normalized to WT/Sv condition, derived from the western analyses shown in (A) and repeats. N = 3.

(D) Mean band densities of pMlc2 relative to total Mlc and normalized to WT/St, derived from the western analyses shown in (B) and repeats. N = 3.

(E) RhoA/C-ROCK signaling pathway. Molecules with putative (Scansite 3.0) or published 14-3-3 binding sites are in red.

(legend continued on next page)

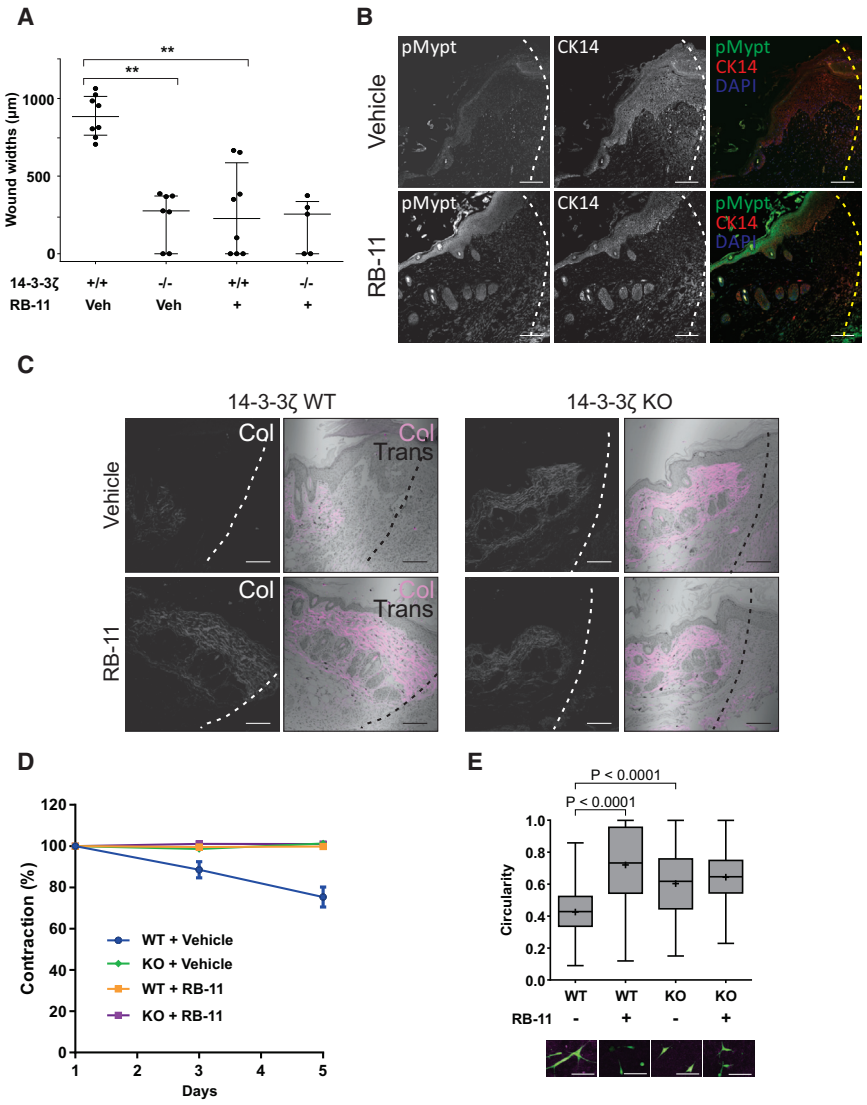

Figure 6. Pharmacological Inhibition of 14-3-3 Accelerates Wound Healing and Phenocopies 14-3-3ζ Deficiency

(A) Wound widths (day 7) of WT or 14-3-3ζ KO mice treated with RB-11 or vehicle control.

(B) Confocal immunofluorescence analysis of p(Thr-696)Mypt1 (green) in WT mice treated with RB-11 or vehicle control. CK14 (red) delineates epidermis. The scale bars represent 100 μm.

(C) Dual two-photon SHG and transmission microscopy (Trans; grayscale in merged) showing collagen (Col; white in single channel, magenta in merged) of H&E-stained sections of wound margins of WT and 14-3-3ζ KO mice treated with RB-11 or vehicle. The scale bars represent 100 μm.

(D) Percentage contraction of collagen matrices from Figure S5 over time. Measurements are shown for WT cells (blue line), WT cells in RB-11 (10 μM, orange line), 14-3-3ζ KO cells (green line), and 14-3-3ζ KO cells in RB-11 (10 μM, purple line). Medium was replenished on day 5. N = 3 matrices per condition.

(E) Cell circularity of WT and 14-3-3ζ KO dermal fibroblasts cultured in collagen matrices with RB-11 (10 μM) or vehicle. N = 3 matrices per condition. Images show single frames from live-cell videos (Movie S2) of dual two-photon GFP-fluorescence (green) and collagen SHG (magenta) analysis of GFP-labeled WT and 14-3-3ζ KO dermal fibroblasts. The scale bars represent 100 μm.

See also Figure S5.

analysis revealed that WT dermal fibroblasts cultured in the presence of RB-11 exhibited a rounded morphology similar to that of 14-3-3ζ KO dermal fibroblasts (Figure 6E) and that treatment with RB-11 caused no further change in the morphology of 14-3-3ζ KO dermal fibroblasts, consistent with the observation that RB-11 inhibited the ability of 14-3-3ζ to interact with Mypt1 (Figures S5B and S5C).

Taken together, these results show that pharmacological inhibition of 14-3-3 phenocopies 14-3-3ζ deficiency, increasing signal flux through the ROCK pathway, impairing the ECM remodeling, and accelerating wound healing.

14-3-3ζ Is Upregulated in Chronic Wounds and Downregulated in Cutaneous SCCs

To determine if 14-3-3ζ-mediated regulation of ROCK signaling has clinical relevance, we performed confocal immunofluorescence analysis of 14-3-3ζ in histological samples of three different categories of patient wounds with long healing times (burn, hypertrophic scar, and diabetic ulcer) and compared these results with those from normal skin. Area coverage analysis of 14-3-3ζ immunofluorescence revealed that diabetic ulcers and hypertrophic scars exhibited >2-fold higher median levels of 14-3-3ζ compared with normal unwounded skin (Figures 7A and S6A). Whereas the majority of burn biopsies expressed high levels of 14-3-3ζ compared with normal skin, the difference was not statistically significant as a proportion of burn samples had levels of 14-3-3ζ that were comparable with that in unwounded skin (Figure 7A). These data suggest that long healing times may arise from increased levels of

(F) Western analysis (WB) of GST-14-3-3ζ Sepharose or GST-Sepharose pull-downs (PD) from WT and 14-3-3ζ KO dermal fibroblast lysates. Antibodies used for WB are on the left, and beads used for PD are on the right. Analysis of 10% of whole-cell extract (WCE) used in the PD experiment is also shown.

(G) Co-immunoprecipitation (IP) analysis of primary dermal fibroblast lysates with G1-7 anti-14-3-3 antibody (isoform non-selective; see Table S1) and the 14-3-3ζ-selective commercial antibody C-16, with and without added phosphatase (C-16$_{(P)}$). Input is 10% of the WCE used per immunoprecipitation.

(H) IP analysis of primary keratinocyte lysates with the 14-3-3ζ selective commercial antibody C-16.

(I) IP analysis of lysates derived from HEK293T cells expressing constructs encoding FLAG-tagged versions of WT Mypt1, Mypt1^{S445A}, Mypt1^{S472A}, Mypt1^{S909A}, or Mypt1 containing all three mutations (Mypt1^{SiiiA}), with anti-FLAG antibody. IgG immunoprecipitation controls are shown at the bottom. Histogram shows 14-3-3ζ band densities from FLAG immunoprecipitation expressed relative to Mypt1 and normalized to WT.

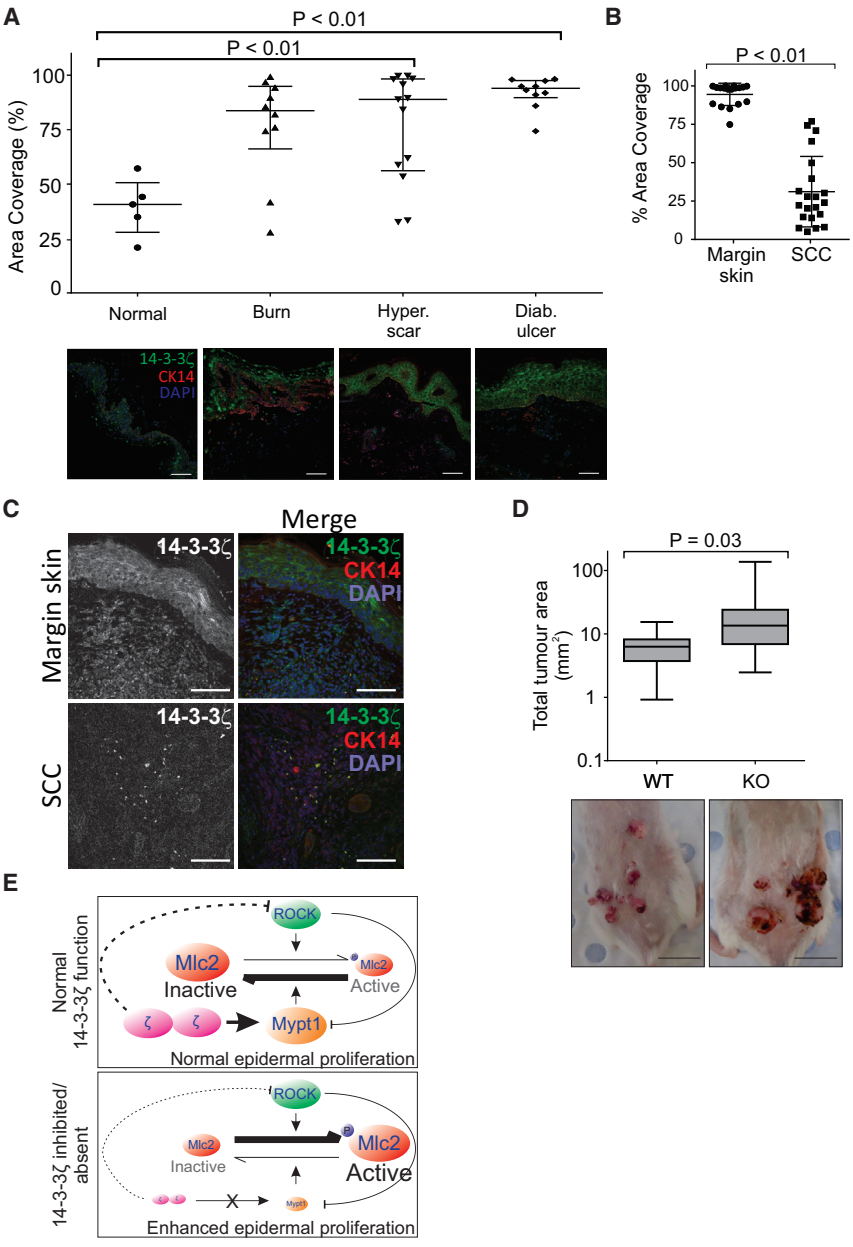

Figure 7. 14-3-3ζ Is Differentially Regulated in Chronic Wounds and Cutaneous SCC

(A) Representative immunofluorescence of 14-3-3ζ (green) in normal human skin (n = 5) and patient wound tissue together with area coverage analysis quantifying 14-3-3ζ levels in wound tissue compared with normal skin, shown as medians and inter-quartile ranges. Burn, burn wound (n = 10); Hyper. scar, hypertrophic scar (n = 13); Diab. ulcer, diabetic ulcer (n = 10). The scale bar represents 100 μm.

(B and C) (B) Area coverage quantification of 14-3-3ζ immunofluorescence (grayscale in monochrome, green in merged) in normal margin skin and cutaneous SCCs from human patients (n = 21), shown as medians and inter-quartile ranges. Representative specimens are shown in (C). The scale bar represents 100 μm.

(D) Median cross-sectional area of tumors in WT and 14-3-3ζ KO mice (ten mice/genotype). Medians and quartiles are shown. Representative images are shown. The scale bar represents 1 cm.

(E) Schematic demonstrating how 14-3-3ζ regulates the equilibrium between the phosphorylated (active) and non-phosphorylated (inactive) versions of Mlc2 by indirectly regulating signal flux through ROCK (dotted line).

See also Figure S6.

14-3-3ζ, which likely results in attenuated ROCK signaling, and that patients with these wounds may therefore benefit from therapy to inhibit 14-3-3 to promote faster re-epithelialization.

Cutaneous SCCs exhibit enhanced mechano-reciprocity characterized by progressively elevated ECM stiffness and ROCK pathway activation (Ibbetson et al., 2013; Samuel et al., 2011a; Samuel and Olson, 2011). To determine the status of 14-3-3ζ-mediated negative regulation of ROCK signaling in cutaneous SCCs, we performed immunofluorescence analysis of 14-3-3ζ in 21 human SCCs and normal margin skin that we have previously characterized in respect of ROCK activation status and ECM protein levels (Ibbetson et al., 2013). 14-3-3ζ is downregulated in a large majority of cutaneous SCCs (Figures 7B and 7C), suggesting that signaling flux downstream of ROCK is no longer moderated by 14-3-3ζ in SCCs, consistent with increased MYPT phosphorylation and elevated collagen and other ECM proteins found in these SCCs (Ibbetson et al., 2013).

To determine the effect of mechano-reciprocity on tumor growth, we next examined tumor size in cohorts of 14-3-3ζ KO and WT mice placed on the two-stage chemical carcinogenesis protocol. Whereas syngeneic papillomas of squamous cell origin arose in both 14-3-3ζ KO and WT mice in similar numbers, 14-3-3ζ KO mice exhibited a significantly larger median papilloma size than WT mice at 30 weeks (Figure 7D) and increased collagen in the tumor stroma (Figure S6B). Taken together with our observations on wound healing in 14-3-3ζ-deficient mice and mice in which 14-3-3 has been pharmacologically inhibited, these observations strongly suggest that 14-3-3ζ-mediated moderation of mechano-reciprocity has an important function in maintaining epidermal homeostasis, by moderating the speed of wound healing and suppressing the growth of epidermal tumors.

DISCUSSION

Re-establishment and remodeling of dermal ECM is a key outcome of wound healing (Li et al., 2007). Given the ECM's role in extra-cellular force generation and because we had previously shown that the ROCK signaling pathway regulates dermal ECM production, we reasoned that important negative regulatory mechanisms identified in this non-transformed system

may have useful implications for diseases of aberrant tissue homeostasis, including cancer.

Signaling through ROCK is enhanced at wound margins throughout healing, resulting in increased production and impaired remodeling of collagen, and elevated periostin and tenascin-C, key ECM proteins whose functions include stiffening the matrix and forming the substratum on which re-epithelialization can occur. However, flux through the ROCK pathway is moderated by 14-3-3ζ, which alone of all its family members is upregulated at wound margins (Figures 1D and 1E), and whose binding of Mypt1 via pSer-909 is associated with de-phosphorylation and inactivation of the regulatory myosin light chain (Mlc2). However, residual 14-3-3ζ binding to Mypt1^{S909A} and Mypt1^{SiiiA} forms of Mypt1 (Figure 5H) suggests that phosphorylation at Serine-909 is not the sole regulator of 14-3-3ζ binding. Indeed, 14-3-3 proteins usually require paired target sites for robust association with client proteins. Because only one of three putative 14-3-3 binding sites on Mypt1 is indispensable for 14-3-3ζ binding, the second site is likely either a non-canonical phospho-amino acid or a hybrid prenyl binding site similar to that recently reported (Riou et al., 2013).

Mlc2 exists in equilibrium between the (active) version pp(Thr-18/Ser-19) phosphorylated by ROCK and the (inactive) non-phosphorylated version. Because the equilibrium between the active and inactive versions of Mlc2 controls actomyosin contractility, Mlc2 inactivation by 14-3-3ζ via Mypt1 reduces actomyosin contractility and the ability of cells to act mechano-reciprocally. 14-3-3ζ therefore negatively regulates mechano-reciprocity, and its mRNA and protein levels are elevated to accomplish this function, consistent with a recent report of transcriptional regulation of YWHAZ gene expression (Kasinski et al., 2014).

14-3-3β has been proposed to dissociate Mypt1 from myosin II and inhibit dephosphorylation of Mlc2 (Koga and Ikebe, 2008). This contrasts with our data that Mlc2 phosphorylation is elevated when 14-3-3ζ is absent (Figures 2I and 2H in keratinocytes and Figure 5B in dermal fibroblasts). It follows that the cellular context greatly influences 14-3-3 function, or that 14-3-3ζ and 14-3-3β have opposing isoform-specific functions. Interestingly, we did not observe co-regulation of these isoforms (Figures S1C and S1F). Although Ser-472 on MYPT1 was reported to be essential for binding 14-3-3β in cell lines (Koga and Ikebe, 2008), we show that phosphorylation at Ser-909 regulates 14-3-3ζ binding and that Ser-472 is dispensable for 14-3-3ζ binding to Mypt1 in the skin (Figure 5H). Further work remains to identify the kinase(s) regulating Mypt1 phosphorylation at Ser-909 in this context and determine how 14-3-3ζ promotes Mypt1 activity. However, our observation that the inactivating phosphorylation of Mypt1 at Thr-696 by ROCK is increased in 14-3-3ζ KO or RB-11 treated tissues and cells (Figures 2F, 2G, 5A, and 6B) strongly suggests that Mypt1 is rendered more susceptible to phosphorylation by ROCK when 14-3-3ζ is absent or inhibited, which is also consistent with increased active pMlc2 under these conditions (Figures 2H, 2I, 5B, and 5D). Our data raise the possibility that upon binding Mypt1, 14-3-3ζ may sterically hinder the interaction with ROCK (a large protein), thereby protecting Mypt1 from phosphorylation and inactivation, while having no effect on its interaction with Mlc2 (a small protein).

Reconstituting 14-3-3ζ KO mice with WT bone marrow failed to return wound healing speed and tissue morphology to normal (Figure 4A), showing that 14-3-3ζ's modulation of healing is independent of the immune system and that the well-known functions of the immune system in wound healing are likely not conducted through 14-3-3ζ.

We propose that keratinocytes in which signaling downstream of ROCK is enhanced by deletion or inhibition of 14-3-3ζ or by direct conditional ROCK activation signal to dermal fibroblasts to increase their ECM production (Figures 3H, 3I, S3B, and S3C), consistent with our previous observations in vivo (Ibbetson et al., 2013; Samuel et al., 2011a). Furthermore, when signaling downstream of ROCK is enhanced in fibroblasts by the same means, the motility of dermal fibroblasts is compromised (Figures 4G, S4C, and S4D; Movie S2) by larger and stable focal adhesions (Movie S1; Figures 4C and 4E), and they are no longer able to remodel collagen in vitro (Figures 4B, 6D, and S5A) or at wound margins in vivo (Figures 2A–2C and 6C), further contributing to increased dermal stiffness. Therefore, loss of 14-3-3ζ activity and increased skin stiffness leads to mechano-reciprocal activation of the integrin → FAK → PI3K/AKT mechano-transduction pathway (Figures 3D–3F). We and others have shown that across many tissue types, increased ECM production elevates stiffness and promotes cell proliferation through this mechano-transduction pathway (Levental et al., 2009; Samuel et al., 2011a), providing a mechanism for rapid wound healing under these conditions.

That 14-3-3ζ KO and RB-11 treated WT mice exhibited comparable wound healing times and that treatment of 14-3-3ζ KO wounds with RB-11 did not accelerate wound healing (Figure 6A) constitute strong circumstantial evidence that acceleration of wound healing by RB-11 results predominantly from the inhibition of 14-3-3ζ. Together with our observation that the 14-3-3ζ isoform alone is upregulated in wounds, these data suggest a non-redundant function of 14-3-3ζ in moderating signaling flux through the ROCK pathway and regulating mechano-reciprocity in the skin.

This raises the question as to why a mechanism to moderate re-epithelialization is required, when it would appear that speedy wound healing would have the significant advantages of rapidly re-establishing skin barrier function and minimizing the risk of infection. However, our data that skin tumor growth is accelerated in 14-3-3ζ KO mice compared with WT mice (Figure 7D) and that 14-3-3ζ is downregulated in human cutaneous SCCs (Figure 7B) lead us to conclude that 14-3-3ζ has a role in maintaining mechano-reciprocity within acceptable boundaries such that re-epithelialization is promoted and tumor growth is not. We propose that in chronic wounds, overexpression of 14-3-3ζ leads to aberrant and persistent downregulation of signaling downstream of ROCK, resulting in a scant and pliant ECM that is incapable of initiating the robust mechanical signal required for re-epithelialization, whereas in cutaneous SCCs, 14-3-3ζ deficiency leads to aberrant and elevated signaling downstream of ROCK, causing increased production of collagen and other molecules that stiffen the matrix and promote keratinocyte proliferation and tumor progression (summarized in Figure 7E). 14-3-3ζ therefore maintains mitogenic mechano-transduction signaling in the skin between healthy boundaries. The need for this balance is illustrated by Marjolin's

ulcer, a form of cutaneous SCC that arises in scar tissue (Saaiq and Ashraf, 2014). The observation that 14-3-3ζ is downregulated in cutaneous SCC contrasts with previous reports that 14-3-3ζ expression is elevated in some other cancers and 14-3-3 has in fact has been proposed as a potential cancer target (Matta et al., 2012). We would therefore sound a note of caution because of the potential pleiotropy of 14-3-3ζ, whose inhibition to target other cancers may promote progression of cutaneous SCCs.

EXPERIMENTAL PROCEDURES

Mice

All procedures were approved by the relevant institutional animal ethics committees. 14-3-3ζ-deficient (Cheah et al., 2012) and K14-ROCK:ER and K14-KD:ER (Samuel et al., 2009a) mice have been previously described.

Incisional Wounding

Incisional wounding was performed as we have previously described (Lees et al., 2013). Daily topical treatments per mouse were as follows: RB-11, 10 μg (25 nmol); Y-27632, 25 μg; and 4HT, 50 μg. Mice were euthanized at relevant time points (2, 5, 7, 14, and 21 days). One wound, with a 1 cm margin, was fixed in 4% formalin O/N at 4°C. Fixed wounds were bisected at the center, processed, and embedded in paraffin. Wound widths were measured on images of H&E-stained sections acquired with NDPView slide scanning and image quantification software. Remaining wounds were processed for molecular analyses.

Chemical Carcinogenesis and Epidermal Hyper-proliferation

Chemical carcinogenesis was performed as we have previously described (Samuel et al., 2011a). Hyper-proliferation was induced with TPA alone.

Cells

Primary murine dermal fibroblasts and keratinocytes were derived as described previously (Calvo et al., 2013; Samuel et al., 2009a). Dermal fibroblasts were transfected with plasmid encoding eGFP-paxillin (Addgene) using Lipofectamine 2000 (Thermo Fisher Scientific) according to the manufacturer's instructions, or infected with retrovirus encoding eGFP (LMP-puro-eGFP) (Dickins et al., 2005) or mCherry (LMP-puro-mCherry) for live-cell imaging. Fibroblasts were starved for 24 hr in serum-free DMEM to minimize Rho-ROCK signaling and stimulated with serum-containing medium supplemented with epidermal growth factor (EGF, 50 ng/ml) for 10 min to 2 hr to stimulate Rho-ROCK signaling (time course in Figure S2K).

Histological and Immunohistological Analyses

Histology and immunohistology were performed as previously described (Ibbetson et al., 2013; Samuel et al., 2009b, 2011a, 2011b). Antigen retrieval buffer, method, and antibody dilutions appear in Table S1. Histology slides were imaged using a Hamamatsu Nanozoomer NDP slide scanner (Hamamatsu Photonics) and Digital Slide Server (Slidepath) software. Transmission and SHG images were acquired simultaneously using an LSM 710 two-photon excitation microscope (Zeiss). Immunofluorescence images were acquired using an LSM 700 confocal microscope (Zeiss).

In all images of sectioned wounds, we have adhered to the following convention: dotted lines indicate wound edges (Figure S2A). Wound margin tissue is to the left of each dotted line.

Bone Marrow Chimeric Mice

Recipient female BALB/c mice (≥8 wk old) were given 750 cGy γ-irradiation from a linear accelerator. One day post-irradiation, mice were engrafted by tail vein injection with female bone marrow cells (WT into WT recipients as irradiation control; KO into WT or WT into KO recipients) using the CD45.1 and CD45.2 to distinguish donor from recipient cells at endpoint. Cells from one donor mouse repopulated three recipients. After 4 weeks in sterile conditions, mice were wounded.

Human Tissue Samples

For human wound and cutaneous SCC samples, informed consent was obtained from patients. Study protocols conformed to ethical guidelines of the 1975 Declaration of Helsinki, reflected in approvals by the Health Service Human Research Ethics Committee and Central Northern Adelaide Health Service Ethics of Human Research Committee approvals HREC/12/TQEHLMH/107, CNAH 11-CHREC-F007, and RAH 120113.

Statistical Analyses

Box-and-whisker plots show medians and quartiles or inter-quartile ranges of non-parametric data, with p values calculated by either the Kruskal-Wallis (three or more groups) or Mann-Whitney (two groups) test with Dunnet's post hoc test. Histograms and line graphs show means and SEs of data exhibiting a normal distribution and were analyzed using Student's t test or ANOVA with Tukey's post-test. $P < 0.05$ was used as the significance cutoff.

SUPPLEMENTAL INFORMATION

Supplemental Information includes Supplemental Experimental Procedures, six figures, one table, and two movies and can be found with this article online at http://dx.doi.org/10.1016/j.devcel.2015.11.026.

AUTHOR CONTRIBUTIONS

H.S.R., A.F.L., and M.S.S. conceived the study. J.K., K.G.S., F.C.S., and M.S.S. performed biochemical analyses. K.G.S., N.T.P., and M.S.S. performed immunohistological analyses. Wound healing studies were performed by R.L.W., J.K., and M.S.S. under the guidance of A.J.C. M.S.S. and A.N.P. performed inhibitor treatments under the guidance of J.M.W. H.S.R performed bone marrow engraftments. N.K. and M.A.G. performed flow cytometry; P.A.M. and S.M.P. designed and performed point mutageneses. A.H.A., A.M., and L.W. performed collagen remodeling and computations analyses under the guidance of P.T. M.S.S. wrote the paper.

ACKNOWLEDGEMENTS

This work was supported by the NHMRC, Australia (M.S.S., H.S.R., A.F.L., A.J.C., P.T., S.M.P., M.A.G.), the ARC (M.S.S., P.T.), the Cancer Councils of South Australia (M.S.S., M.A.G., S.M.P., H.S.R.) and New South Wales (P.T.), the Cancer Institute New South Wales (A.M.) and the Royal Adelaide Hospital Research Fund (M.S.S.). H.S.R. is the Peter Nelson Leukemia Research Fellow of the Cancer Council of South Australia. The authors acknowledge the support of donors to the Health Services Charitable Gifts Board (HSCGB) of South Australia, which supported the purchase of some of the imaging equipment. We thank Prof. Geoff Hill (QIMR Berghofer Medical Research Institute) for the gift of CD45.1 BALB/c mice and Dr. Sarah Boyle for critical reading of the manuscript.

Received: January 20, 2015
Revised: September 23, 2015
Accepted: November 23, 2015
Published: December 21, 2015

REFERENCES

Aitken, A. (2006). 14-3-3 proteins: a historic overview. Semin. Cancer Biol. *16*, 162–172.

Amano, M., Ito, M., Kimura, K., Fukata, Y., Chihara, K., Nakano, T., Matsuura, Y., and Kaibuchi, K. (1996). Phosphorylation and activation of myosin by Rho-associated kinase (Rho-kinase). J. Biol. Chem. *271*, 20246–20249.

Assoian, R.K., and Klein, E.A. (2008). Growth control by intracellular tension and extracellular stiffness. Trends Cell Biol. *18*, 347–352.

Bainbridge, P. (2013). Wound healing and the role of fibroblasts. J. Wound Care *22*, 407–408, 410–412.

Burridge, K., and Wennerberg, K. (2004). Rho and Rac take center stage. Cell *116*, 167–179.

Butcher, D.T., Alliston, T., and Weaver, V.M. (2009). A tense situation: forcing tumour progression. Nat. Rev. Cancer *9*, 108–122.

Calvo, F., Ege, N., Grande-Garcia, A., Hooper, S., Jenkins, R.P., Chaudhry, S.I., Harrington, K., Williamson, P., Moeendarbary, E., Charras, G., and Sahai, E. (2013). Mechanotransduction and YAP-dependent matrix remodelling is required for the generation and maintenance of cancer-associated fibroblasts. Nat. Cell Biol. *15*, 637–646.

Cheah, P.S., Ramshaw, H.S., Thomas, P.Q., Toyo-Oka, K., Xu, X., Martin, S., Coyle, P., Guthridge, M.A., Stomski, F., van den Buuse, M., et al. (2012). Neurodevelopmental and neuropsychiatric behaviour defects arise from 14-3-3ζ deficiency. Mol. Psychiatry *17*, 451–466.

Cowin, A.J., Hatzirodos, N., Teusner, J.T., and Belford, D.A. (2003). Differential effect of wounding on actin and its associated proteins, paxillin and gelsolin, in fetal skin explants. J. Invest. Dermatol. *120*, 1118–1129.

Darby, I., Skalli, O., and Gabbiani, G. (1990). Alpha-smooth muscle actin is transiently expressed by myofibroblasts during experimental wound healing. Lab. Invest. *63*, 21–29.

Dickins, R.A., Hemann, M.T., Zilfou, J.T., Simpson, D.R., Ibarra, I., Hannon, G.J., and Lowe, S.W. (2005). Probing tumor phenotypes using stable and regulated synthetic microRNA precursors. Nat. Genet. *37*, 1289–1295.

Driskell, R.R., and Watt, F.M. (2015). Understanding fibroblast heterogeneity in the skin. Trends Cell Biol. *25*, 92–99.

Egeblad, M., Rasch, M.G., and Weaver, V.M. (2010). Dynamic interplay between the collagen scaffold and tumor evolution. Curr. Opin. Cell Biol. *22*, 697–706.

Eming, S.A., Krieg, T., and Davidson, J.M. (2007). Inflammation in wound repair: molecular and cellular mechanisms. J. Invest. Dermatol. *127*, 514–525.

Feng, J., Ito, M., Ichikawa, K., Isaka, N., Nishikawa, M., Hartshorne, D.J., and Nakano, T. (1999). Inhibitory phosphorylation site for Rho-associated kinase on smooth muscle myosin phosphatase. J. Biol. Chem. *274*, 37385–37390.

Haydont, V., Bourgier, C., Pocard, M., Lusinchi, A., Aigueperse, J., Mathé, D., Bourhis, J., and Vozenin-Brotons, M.C. (2007). Pravastatin Inhibits the Rho/CCN2/extracellular matrix cascade in human fibrosis explants and improves radiation-induced intestinal fibrosis in rats. Clin. Cancer Res. *13*, 5331–5340.

Ibbetson, S.J., Pyne, N.T., Pollard, A.N., Olson, M.F., and Samuel, M.S. (2013). Mechanotransduction pathways promoting tumor progression are activated in invasive human squamous cell carcinoma. Am. J. Pathol. *183*, 930–937.

Ichimura, T., Isobe, T., Okuyama, T., Takahashi, N., Araki, K., Kuwano, R., and Takahashi, Y. (1988). Molecular cloning of cDNA coding for brain-specific 14-3-3 protein, a protein kinase-dependent activator of tyrosine and tryptophan hydroxylases. Proc. Natl. Acad. Sci. U S A *85*, 7084–7088.

Kasinski, A., Dong, X., Khuri, F.R., Boss, J., and Fu, H. (2014). Transcriptional regulation of YWHAZ, the gene encoding 14-3-3ζ. PLoS ONE *9*, e93480.

Koga, Y., and Ikebe, M. (2008). A novel regulatory mechanism of myosin light chain phosphorylation via binding of 14-3-3 to myosin phosphatase. Mol. Biol. Cell *19*, 1062–1071.

Kudo, A. (2011). Periostin in fibrillogenesis for tissue regeneration: periostin actions inside and outside the cell. Cell. Mol. Life Sci. *68*, 3201–3207.

Lees, J.G., Ching, Y.W., Adams, D.H., Bach, C.T., Samuel, M.S., Kee, A.J., Hardeman, E.C., Gunning, P., Cowin, A.J., and O'Neill, G.M. (2013). Tropomyosin regulates cell migration during skin wound healing. J. Invest. Dermatol. *133*, 1330–1339.

Levental, K.R., Yu, H., Kass, L., Lakins, J.N., Egeblad, M., Erler, J.T., Fong, S.F., Csiszar, K., Giaccia, A., Weninger, W., et al. (2009). Matrix crosslinking forces tumor progression by enhancing integrin signaling. Cell *139*, 891–906.

Li, J., Chen, J., and Kirsner, R. (2007). Pathophysiology of acute wound healing. Clin. Dermatol. *25*, 9–18.

Maller, O., DuFort, C.C., and Weaver, V.M. (2013). YAP forces fibroblasts to feel the tension. Nat. Cell Biol. *15*, 570–572.

Matta, A., Siu, K.W., and Ralhan, R. (2012). 14-3-3 zeta as novel molecular target for cancer therapy. Expert Opin. Ther. Targets *16*, 515–523.

McGrail, D.J., Kieu, Q.M., and Dawson, M.R. (2014). The malignancy of metastatic ovarian cancer cells is increased on soft matrices through a mechanosensitive Rho-ROCK pathway. J. Cell Sci. *127*, 2621–2626.

Messaritou, G., Grammenoudi, S., and Skoulakis, E.M. (2010). Dimerization is essential for 14-3-3zeta stability and function in vivo. J. Biol. Chem. *285*, 1692–1700.

Midwood, K.S., Hussenet, T., Langlois, B., and Orend, G. (2011). Advances in tenascin-C biology. Cell. Mol. Life Sci. *68*, 3175–3199.

Niedel, J.E., Kuhn, L.J., and Vandenbark, G.R. (1983). Phorbol diester receptor copurifies with protein kinase C. Proc. Natl. Acad. Sci. U S A *80*, 36–40.

Nobis, M., McGhee, E.J., Morton, J.P., Schwarz, J.P., Karim, S.A., Quinn, J., Edward, M., Campbell, A.D., McGarry, L.C., Evans, T.R., et al. (2013). Intravital FLIM-FRET imaging reveals dasatinib-induced spatial control of src in pancreatic cancer. Cancer Res. *73*, 4674–4686.

Obenauer, J.C., Cantley, L.C., and Yaffe, M.B. (2003). Scansite 2.0: Proteome-wide prediction of cell signaling interactions using short sequence motifs. Nucleic Acids Res. *31*, 3635–3641.

Olsen, J.V., Vermeulen, M., Santamaria, A., Kumar, C., Miller, M.L., Jensen, L.J., Gnad, F., Cox, J., Jensen, T.S., Nigg, E.A., et al. (2010). Quantitative phosphoproteomics reveals widespread full phosphorylation site occupancy during mitosis. Sci. Signal. *3*, ra3.

Ramshaw, H., Xu, X., Jaehne, E.J., McCarthy, P., Greenberg, Z., Saleh, E., McClure, B., Woodcock, J., Kabbara, S., Wiszniak, S., et al. (2013). Locomotor hyperactivity in 14-3-3ζ KO mice is associated with dopamine transporter dysfunction. Transl. Psychiatry *3*, e327.

Riou, P., Kjær, S., Garg, R., Purkiss, A., George, R., Cain, R.J., Bineva, G., Reymond, N., McColl, B., Thompson, A.J., et al. (2013). 14-3-3 proteins interact with a hybrid prenyl-phosphorylation motif to inhibit G proteins. Cell *153*, 640–653.

Russo, J.M., Florian, P., Shen, L., Graham, W.V., Tretiakova, M.S., Gitter, A.H., Mrsny, R.J., and Turner, J.R. (2005). Distinct temporal-spatial roles for rho kinase and myosin light chain kinase in epithelial purse-string wound closure. Gastroenterology *128*, 987–1001.

Saaiq, M., and Ashraf, B. (2014). Marjolin's ulcers in the post-burned lesions and scars. World J. Clin. Cases *2*, 507–514.

Samuel, M.S., and Olson, M.F. (2011). Actomyosin contractililty: force power drives tumor growth. Cell Cycle *10*, 3409–3410.

Samuel, M.S., Munro, J., Bryson, S., Forrow, S., Stevenson, D., and Olson, M.F. (2009a). Tissue selective expression of conditionally-regulated ROCK by gene targeting to a defined locus. Genesis *47*, 440–446.

Samuel, M.S., Suzuki, H., Buchert, M., Putoczki, T.L., Tebbutt, N.C., Lundgren-May, T., Christou, A., Inglese, M., Toyota, M., Heath, J.K., et al. (2009b). Elevated Dnmt3a activity promotes polyposis in Apc(Min) mice by relaxing extracellular restraints on Wnt signaling. Gastroenterology *137*, 902–913.

Samuel, M.S., Lopez, J.I., McGhee, E.J., Croft, D.R., Strachan, D., Timpson, P., Munro, J., Schröder, E., Zhou, J., Brunton, V.G., et al. (2011a). Actomyosin-mediated cellular tension drives increased tissue stiffness and β-catenin activation to induce epidermal hyperplasia and tumor growth. Cancer Cell *19*, 776–791.

Samuel, M.S., Lourenço, F.C., and Olson, M.F. (2011b). K-Ras mediated murine epidermal tumorigenesis is dependent upon and associated with elevated Rac1 activity. PLoS ONE *6*, e17143.

Schultz, G.S., Davidson, J.M., Kirsner, R.S., Bornstein, P., and Herman, I.M. (2011). Dynamic reciprocity in the wound microenvironment. Wound Rep. Regen. *19*, 134–148.

Tian, B., Lessan, K., Kahm, J., Kleidon, J., and Henke, C. (2002). Beta 1 integrin regulates fibroblast viability during collagen matrix contraction through a phosphatidylinositol 3-kinase/Akt/protein kinase B signaling pathway. J. Biol. Chem. *277*, 24667–24675.

Timpson, P., McGhee, E.J., Erami, Z., Nobis, M., Quinn, J.A., Edward, M., and Anderson, K.I. (2011). Organotypic collagen I assay: a malleable platform to assess cell behaviour in a 3-dimensional context. J. Vis. Exp. *56*, e3089.

Toker, A., Sellers, L.A., Amess, B., Patel, Y., Harris, A., and Aitken, A. (1992). Multiple isoforms of a protein kinase C inhibitor (KCIP-1/14-3-3) from sheep brain. Amino acid sequence of phosphorylated forms. Eur. J. Biochem. *206*, 453–461.

Tomasek, J.J., Gabbiani, G., Hinz, B., Chaponnier, C., and Brown, R.A. (2002). Myofibroblasts and mechano-regulation of connective tissue remodelling. Nat. Rev. Mol. Cell Biol. *3*, 349–363.

Uhart, M., and Bustos, D.M. (2013). Human 14-3-3 paralogs differences uncovered by cross-talk of phosphorylation and lysine acetylation. PLoS ONE *8*, e55703.

Wang, J., Zhang, Y., Zhang, N., Wang, C., Herrler, T., and Li, Q. (2015). An updated review of mechanotransduction in skin disorders: transcriptional regulators, ion channels, and microRNAs. Cell. Mol. Life Sci. *72*, 2091–2106.

Wilkinson, S., Paterson, H.F., and Marshall, C.J. (2005). Cdc42-MRCK and Rho-ROCK signalling cooperate in myosin phosphorylation and cell invasion. Nat. Cell Biol. *7*, 255–261.

Wong, V.W., Longaker, M.T., and Gurtner, G.C. (2012). Soft tissue mechanotransduction in wound healing and fibrosis. Semin. Cell Dev. Biol. *23*, 981–986.

Woodcock, J.M., Ma, Y., Coolen, C., Pham, D., Jones, C., Lopez, A.F., and Pitson, S.M. (2010). Sphingosine and FTY720 directly bind pro-survival 14-3-3 proteins to regulate their function. Cell. Signal. *22*, 1291–1299.

Woodcock, J.M., Coolen, C., Goodwin, K.L., Baek, D.J., Bittman, R., Samuel, M.S., Pitson, S.M., and Lopez, A.F. (2015). Destabilisation of dimeric 14-3-3 proteins as a novel approach to anti-cancer therapeutics. Oncotarget *6*, 14522–14536.